Effect of tin filter-based spectral shaping CT on image quality and radiation dose for routine use on ultralow-dose CT protocols: A phantom study

J. Greffier, F. Pereira, A. Hamard, T. Addala, J.P. Beregi, J. Frandon

Effect of tin filter-based spectral shaping CT on image quality and radiation dose for routine use on ultralow-dose CT protocols: a phantom study

Short title:

Effect of tin filter on image quality and radiation dose

J. GREFFIER[1*], F. PEREIRA[1], A. HAMARD[1], T. ADDALA[1], J.P. BEREGI[1], J. FRANDON[1]

Affiliations

All authors [1]Department of Radiology, CHU Nîmes, Univ Montpellier, Medical Imaging Group Nîmes, EA 2415, 30029 Nîmes, France

* Corresponding author: joel.greffier@chu-nimes.fr

Department of Radiolgy, CHU de Nîmes, Medical Imaging Group Nîmes, EA 2415, Bd Prof Robert Debré, 30029 Nîmes Cedex 9, France

Abstract

Purpose. The purpose of this study was to assess the impact of tin filter (TF) on X-ray beam quality, image quality and radiation dose and its suitability for routine use for chest and lumbar-spine/pelvis-hip ultralow-dose (ULD) CT examination protocols.

Methods. The X-ray beam quality was determined by measuring the half-value layer (HVL) and calculating the mean weighted energy for 100, 120, 150 kVp (using standard filtration) and for 100 and 150 kVp using TF (Sn100 kVp and Sn150 kVp, respectively). Acquisitions were performed on a phantom at four dose levels for each previously defined kVp. The mean attenuation (N_{CT}), noise-power-spectrum (NPS) and task-based transfer function (TTF) were computed. The detectability index (d') was computed to model the detection of two lesions in spine and pelvic/hip examination and two for chest exploration. Image quality and detectability using a TF were assessed for two routinely used ULD protocols.

Results. The HVL and mean weighted energy increased using a TF for the same tube voltage. Using a TF for the same tube voltage changed N_{CT} for bone and acrylic inserts, decreased the NPS peak without changing the NPS spatial frequency and increased the TTF values. The d' values were improved using a TF and with the dose increase. d' values of all modeled lesions were improved using Sn100 kVp and Sn150 kVp for the lumbar-spine/pelvis-hip and chest ULD protocols except for sclerotic bone lesion using Sn150 kVp.

Conclusion. The use of TF increases the X-ray beam quality and improves the image quality characteristics in phantom images represents a promising tool for reducing dose and/or improving the image quality of ULD protocols.

Keywords: Multidetector computed tomography; Image enhancement; Radiation dose; Ultra low dose protocol.

Abbreviations

ADMIRE: advanced modeled iterative reconstruction

CT: computed tomography

$CTDI_{vol}$: volume computed tomography dose index

d': detectability index

ESF: edge-spread function

HVL: half-value layer

IR: iterative reconstruction

LSF: line-spread function

NPS: noise power spectrum

NPWE: non-prewhitening observer model with eye filter

ROI: region of interest

TF: tin filter

TTF: task-based transfer function

ULD: Ultralow dose

Introduction

The dose delivered to a patient during computed tomography (CT) examination is a public health concern [1]. Accordingly, CT protocols should be optimized as much as possible. In this sense, manufacturers are constantly developing tools to reduce the doses delivered to patients while maintaining CT image quality level suitable for diagnosis. The two main tools routinely used to apply this optimization principle are tube current modulation and iterative reconstructions (IR).

Many clinical studies have shown high dose reductions using IR [2-8]. New "ultralow-dose" (ULD) protocols have emerged that are increasingly used in clinical routines. There is no strict definition in the literature for ULD protocols, but their dose levels are close to those of the respective radiographic examination.

ULD protocols are used when the intrinsic contrast between two structures is high. In the literature, ULD protocols exist for the thorax, and protocols for the spine and extremities have begun to appear. The image quality obtained with these ULD protocols is degraded but remains sufficient for the detection of fractures or lytic and sclerotic bone lesions in osteoarticular examinations [9] or for the diagnosis of nontraumatic pneumothorax, pleural or pericardial effusion or pneumonia in a chest examination [7; 10]. However, these ULD protocols cannot be used in overweight patients [6; 7; 10]. Indeed, the quantity and the quality of the X-rays used are not sufficient to traverse these patients, making the image uninterpretable. To compensate for this problem, it would be necessary to increase the tube

voltage and/or to use additional filtration coupled with an increase in tube current (mA), but this is not always possible or available on the CT scanner being used.

All CT systems regardless of the manufacturer are equipped with a sort of pre-filtration, which hardens the beam and absorbs the low-energy photons that increase the dose to the patient without contributing to the final image. This filtration must be designed to support a range of examinations including contrast-enhanced imaging where photons with energies slightly above the k-edge of iodine (33 keV) are preferred. An additional built-in tin filter (TF) has become available on all new CT scanners from Siemens Healthineers. This filter can further harden the beam and increase the mean energy for imaging applications like dual energy CT or non-enhanced CT.

Initial clinical studies on the use of this filter for ULD protocols of the chest, spine and abdomen have been performed [11-15]. The results of these studies show that the use of the TF can greatly reduce doses compared to conventional protocols. However, these studies have not evaluated the impact of tin filter on different image quality metrics.

The aim of this study was to assess the impact of tin filter (TF) on X-ray beam quality, image quality and radiation dose and its suitability for routine use on chest and lumbar-spine/pelvis-hip ULD protocol [9].

Materials and methods

CT system

A third-generation dual-source CT system Somatom Force® (Siemens Healthineers) equipped with the Stellar detectors and the advanced model-based IR (ADMIRE) algorithm was used in this study. Usually, a TF can be used at 150 kVp (with the X-Ray tube "B") for spectral acquisition using a dual-source with two different energies. However, TF is now available at 100 kVp and 150 kVp for a single-source acquisition with a single energy. The use of a TF allows for further hardening of the X-ray beam by reducing the number of low energy photons more effectively than high energy photons, increasing thus the mean energy of the emitted X-ray beam spectrum.

X-ray beam quality assessment

The half-value layer (HVL) was measured to assess the X-ray beam quality obtained with and without a TF. A RaySafe Xi R/F dosimeter (Unfors RaySafe AB) was placed on a

support and centered at the CT scanner isocenter (Fig. 1). This dosimeter and its converter are calibrated in a dosimetry laboratory (Swedish National Testing and Research Institute) for four different beam qualities (50 kVp, 70 kVp, 100 kVp and 150 kVp).

The HVL measurement was performed in "service mode", with X-ray tube "A" at 270° in a fixed position for 100 kVp, 120 kVp, 150 kVp, 100 kVp with TF (Sn100 kVp) and 150 kVp with TF (Sn150 kVp). The other parameters were fixed: tube current at 300 mA and beam collimation at 96×0.6 mm. The HVLs were given in thickness of aluminum (mmAl) by the dosimeter.

A spectrum of photon energies for each kVp was derived by SpeckCalc (McGill University; Montreal, Canada) software (Figure 2) [16]. The mean energy of the X-ray photons ($\bar{E}$) for each spectrum was obtained by performing a weighted mean of the photon intensity values (p_n) as a function of the energy (E_n, keV), as follow:

$$\bar{E} = \frac{p_1 E_1 + p_2 E_{2+\cdots+}p_n E_n}{p_1 + p_2 + \cdots + p_n}$$

Image quality assessment

Acquisition and reconstruction parameters

Acquisitions were performed on a 20 cm-diameter ACR QA phantom (Gammex 464) placed inside a body ring (diameter of 33 cm and length of 24 cm) to more closely simulate the patient's morphology (Figure 3). Five-tube voltages were used, including 100 kVp, 120 kVp, 150 kVp, Sn100 kVp and Sn150 kVp. Tube currents (mAs) were defined to obtain four dose levels: 0.4, 1.5, 2.5 and 3.4 mGy (**Table 1**). It was technically impossible to perform a dose level of 0.4 mGy at 150 kVp. Dose level of 0.4 mGy correspond to the chest ULD protocol (C-ULD) [7; 10] and 3.4 mGy to the lumbar-spine/pelvis-hip ULD protocol (S-ULD) [9] used in our institution.

The raw data were reconstructed using the level 4 of ADMIRE (A4) with the reconstruction kernel "Regular Sharpness" level 40 (Br40, for soft tissue exploration). Images were reconstructed using a slice thickness close to 3 mm (3 mm increments) and a field-of-view of 250 mm. All of these reconstruction parameters correspond to those used routinely in our C-ULD and S-ULD protocols.

Mean attenuation

Mean attenuation assessment was performed using in-house Matlab (MathWorks) routines. Three circular regions of interest (ROI) were placed semi-automatically on module 1 of the ACR phantom in bone (955 HU), acrylic (120 HU), and air inserts (-990 UH) (Figure 3). The mean CT number (N_{CT}) was obtained for the pixels within each ROI.

Task-based image quality assessment

Image quality assessment was carried out using imQuest software (Duke, NC) to assess the noise power spectrum (NPS), the task-based transfer function (TTF) and the detectability index (d') [8].

NPS was computed by placing four square regions of interest (ROIs) in the uniform section (module 3) of the ACR phantom, as follows:

$$NPS_{2D}(f_x, f_y) = \frac{\Delta_x \Delta_y}{L_x L_y} \frac{1}{N_{ROI}} \sum_{i=1}^{N_{ROI}} |FT_{2D}\{ROI_i(x,y) - \overline{ROI_i}\}|^2$$

where Δx and Δy are the pixel size in the x- and y-directions, respectively, Lx and Ly are the ROI size in pixels along the x and y axis, respectively, N_{ROI} is the number of ROIs, FT is the Fourier transform and $\overline{ROI_i}$ is the mean pixel value measured from ROI (x, y) using a first-order detrending technique. The combined NPS was computed on a total of 40 ROIs (N_{ROI}) of 128×128 pixels (L_x and L_y) each, within 10 consecutive axial slices.

The TTF was assessed using three cylindrical inserts available in module 1 of the ACR phantom from seven consecutive axial slices according to the methodology previously reported [17] and used [8]. A circular ROI was placed around the insert, and a circular-edge technique was employed to measure the edge spread function (ESF) by plotting the N_{CT} of each pixel as a function of the distance to the center of the insert. The line spread function (LSF) was then obtained by derivation of the ESF. The TTF was computed from the normalized Fourier transformation of the LSF.

A non-prewhitening observer model with an eye filter (d'$_{NPWE}$) was used to calculate the detectability index:

$$d'^2_{NPWE} = \frac{[\iint |W(u,v)|^2 . TTF(u,v)^2 . E(u,v)^2 du dv]^2}{\iint |W(u,v)|^2 . TTF(u,v)^2 . NPS(u,v)^2 . E(u,v)^4 du dv}$$

where u and v are the spatial frequencies in the x- and y-directions, respectively, E is the eye filter that models the human visual system's sensitivity to different spatial frequencies [18-21], and W (u,v) is the task function defined as:

$$W = |F\{h_1(x,y) - h_2(x,y)\}|$$

where $h_1(x,y)$ and $h_2(x,y)$ correspond to the object present and the object absent hypotheses, respectively.

The eye filter was modeled according to the visual response function [20]. Three task functions assumed to represent a circular signal of 5-mm diameter were simulated in this study. To take into account the N_{CT} variations as a function of kVp, the contrast of each clinical task was defined directly from N_{CT} variations between the insert and the background material of the phantom. We used the results of the N_{CT} and the TTF for the acrylic insert to define a first clinical task simulating a lytic bone lesion [9] and a second task of ground-glass opacities in the lung parenchyma [22]. N_{CT} and TTF outcomes of air insert were used to simulate a clinical task of the detection of a high contrast pulmonary lesion with approximatively 1000 HU between the lung parenchyma and the lesion (such as confluent alveolar opacities, fibrotic lesion, mycetoma formation) and N_{CT} and TTF results of bone insert for the detection of a sclerotic bone lesion [9].

The interpretation conditions used to obtain d' included a zoom factor of 1.5, a viewing distance of 450 mm, and a field of view of 500 mm to refer to the visualization screen.

To assess the potential increase in the detectability index (d') using TF for C-ULD protocol, a comparison of d' value obtained with 100 kVp, Sn100 kVp and Sn 150 kVp at 0.4 mGy was performed. Similar assessments were performed for 120 kVp, Sn100 kVp and Sn 150 kVp at 3.4 mGy for S-ULD protocol.

Dosimetry

Volume CT dose indexes (CTDI$_{vol}$), determined for a 32-cm diameter (polymethyl methacrylate) reference phantom, were retrieved manually from the review report available in the CT workstation at the end of the acquisitions.

Results

X-ray beam quality assessment

The measured HVLs were equal to 7.1 mmAl for 100 kVp, 8.2 mmAl for 120 kVp and 9.5 mmAl for 150 kVp. The HVL increased by 82% with Sn100 kVp (12.9 mmAl) compared to 100 kVp and increased by 64% (15.6 mmAl) with Sn150 kVp compared to 150 kVp.

The mean weighted energy calculated for each spectrum was 58.7 keV for 100 kVp, 64.2 keV for 120 kVp and 72.1 keV for 150 kVp. The mean weighted energy increased by 29% with Sn100 kVp (76.0 keV) compared to 100 kVp and increased by 37% (98.6 keV) with Sn150 kVp compared to 150 kVp.

Mean attenuation

N_{CT} for bone, acrylic and air inserts for each tube voltage at all dose levels are reported in Table 2. N_{CT} was not affected by the tube voltage for air insert. For bone insert, N_{CT} were lower with Sn100 kVp than with 100 kVp (mean: -17 ± 1 [SD] %) and with Sn150 kVp than 150 kVp (mean: -15 ± 0 [SD] %). For acrylic insert, the opposite pattern was found: 6 ± 1 [SD] % and 5 ± 1 [SD] %, respectively.

Task-based image quality assessment

Noise power spectrum

Table 3 reports the NPS peaks and the mean NPS spatial frequency data. Figure 4 shows the NPS curves obtained for all dose levels.

NPS peak values decreased when the dose increased. The NPS peak values at 120 and 150 kVp were in the same range (mean: -2 ± 3 [SD] %) but lower to those obtained at 100 kVp (mean: -11% ± 9 [SD] % and -9 ± 4 [SD] %, respectively). The NPS peak values with Sn100 kVp were lower than with 100 kVp (mean: -36 ± 3 [SD] %). The same pattern was found with Sn150 kVp compared to 150 kVp (mean: -21 ± 7 [SD] %). Finally, the NPS peak was higher with Sn150 kVp than with Sn100 kVp (mean: 8 ± 6 [SD] %).

The mean values of the NPS spatial frequency increased when the dose increased. NPS frequency values were similar for 100 kVp (mean: 0.20 ± 0.01 [SD] mm^{-1}), 120 kVp (mean: 0.20 ± 0.01 [SD] mm^{-1}) and Sn100 kVp (mean: 0.21 ± 0.01 [SD] mm^{-1}). The highest values

were found for 150 kVp (mean: 0.21 ± 0.01 [SD] mm^{-1}) and Sn150 kVp (mean: 0.22 ± 0.01 [SD] mm^{-1}).

Task-based transfer function

The results of the TTF$_{50\%}$ obtained for the three inserts and for the tube voltage as a function of the dose level are presented in Table 4. The TTF decreased as the dose decreased. This reduction was more marked with the acrylic insert than with the two other inserts.

TTF$_{50\%}$ values with Sn150 kVp were higher than with Sn100 kVp for all inserts. TTF$_{50\%}$ values with Sn100 kVp were higher than with 100 kVp for acrylic insert (mean: 14 ± 4 [SD] %) but in the same range for bone (mean: 3 ± 2 [SD] %) and air (mean: 3 ± 0 [SD] %) inserts. TTF$_{50\%}$ values with Sn150 kVp were within the same range than with 150 kVp (mean: 4 ± 2 [SD] % for acrylic insert, mean: 5 ± 0 [SD] % for bone insert and mean: 3 ± 3 [SD] % for air insert).

Detectability index (d')

Values of d' decreased when the dose decreased (Figure 5). The variations of d' values as function of the kVp (without TF) were different according to the simulated lesion. For sclerotic bone lesion, d' decreased as the kVp increased (except at 0.4 mGy). The opposite feature was found for both other simulated lesions.

Compared to 100 kVp, using Sn100 kVp yielded higher d' values, but these variations decreased when the dose increased. The mean increases were 56 ± 23 [SD] % for low contrast lesion, 5 ± 2 [SD] % for the sclerotic bone lesion and 25 ± 2 [SD] % for the high contrast pulmonary lesion.

A similar pattern was found for Sn150 kVp compared to 150 kVp, except for sclerotic bone lesion (mean: -3 ± 2 [SD] %). The mean d' values were higher by in mean 15 ± 3 [SD] % for the high contrast pulmonary lesion and 29 ± 13 [SD] % for low contrast lesion.

Finally, d' values obtained with Sn150 kVp were lower than with Sn100 kVp for the sclerotic bone lesion (mean: -21 ± 2 [SD] % and for the high contrast pulmonary lesion (mean: -1 ± 4 [SD] %) and the opposite for low contrast lesion (mean: 6 ± 6 [SD] %).

Potential increase in the detectability index (d')

Table 5 shows the variations of d' values obtained using Sn100 kVp and Sn150 kVp for both modeled lesions compared to the two ULD protocols evaluated. For the chest ULD protocol, d' values were improved using a TF. This improvement was higher for the ground-glass opacities in the lung parenchyma lesion (using acrylic insert) than the high contrast pulmonary lesion (using air insert). The variation in d' was greater using Sn100 kVp than Sn150 kVp for both lesions.

For the lumbar spine or pelvis/hips ULD protocols, similar improvement of d' values were found using Sn100 kVp and Sn150 kVp for the lytic bone lesion (using acrylic lesion). For sclerotic bone lesion (using bone insert), d' were slightly improved only for Sn100 kVp.

Discussion

This study demonstrates that the use of a TF is of great interest for dose reduction approaches in CT, especially for ULD protocols. Preliminary clinical studies have shown significant dose reductions using a TF for thoracic, abdominopelvic, and spinal explorations [11-15]. However, no study had assessed the impact of a TF on X-ray beam quality or on image quality metrics. For the first time, the present study assesses the impact of a TF on the HVL and on image quality using a task-based assessment [8; 9].

The outcomes of this study showed that the use of a TF changed the photon spectra. The HVL was increased by approximately 82% between 100 kVp and Sn100 kVp and by approximately 64% between 150 kVp and Sn150 kVp. The mean weighted energy calculated for each spectrum also increased between tube voltages with or without a TF. The increases in these two parameters show that the use of a TF further hardens the beam by preferentially absorbing low-energy photons. This behavior may be useful for reducing the dose delivered to patients and for improving the image quality in areas of high attenuation, such as in shoulders, in explorations of the cervical spine [12] or in explorations of the lung apex [11]. However, the outcomes found in this study showed that the hardening of the beam changed the values of N_{CT} for bone and acrylic inserts. For the same voltage, N_{CT} were reduced for the bone insert using TF whereas for the acrylic insert they were increased.

The NPS results found in this study showed that the noise magnitude was reduced using the TF for the same tube voltage. This reduction was greater using Sn100 kVp than using Sn150 kVp. It should also be noted that the NPS peak was higher for Sn150 kVp than for Sn100

kVp. However, the use of a TF weakly influenced the NPS spatial frequency and thus did not appear to change the image texture (such as image smoothness). As also observed in previous studies, the NPS spatial frequency decreased with decreasing dose changing the image texture (smoother image in particular) [2; 3; 23; 24].

The TTF outcomes found in this study showed that the spatial resolution adapted to the clinical task was improved using the TF for the same tube voltage. This improvement in the $TTF_{50\%}$ values was of the same magnitude (range from 0% to 6%) for Sn150 kVp for all inserts and for Sn100 kVp for bone and air inserts. However, a greater improvement was found for Sn100 kVp for the acrylic insert (14±4%). The values of $TTF_{50\%}$ shifted toward a lower frequency when the dose was reduced, regardless of the insert and tube voltage used. Similar results were found in previous studies [8; 25].

The combined variations of N_{CT}, magnitude and texture of noise and TTF have a direct impact on d' values. The improvement of NPS and TTF outcomes leads to higher d' values using a TF for the same voltage for all features (except for sclerotic bone lesion using Sn150 kVp). The variations of N_{CT} as a function of the insert cause different behavior between Sn100 kVp and Sn150 kVp for the different clinical tasks. For lytic bone lesion or pulmonary ground glass opacity, variations of N_{CT} values and TTF outcomes for acrylic insert led to higher d' values with 150 kVp or Sn150 kVp than with 100 kVp or Sn100 kVp. For sclerotic bone lesion, N_{CT} values of bone insert were lower with150kV or Sn150 kVp than with 100 kVp or Sn100 kVp. For similar TTF values and highest NPS outcomes, d' values were higher with 100 kVp or Sn100 kVp than with 150 kVp or Sn150 kVp. For high contrast pulmonary lesion, N_{CT} and TTF outcomes for air insert were not changed as a function of the kVp and d' values were directly linked to the NPS variations according to the kVp, i.e. better with Sn100 kVp than with Sn150 kVp. Finally, similar results for the variation in d' values according to the dose level for the same features were found in the literature [8; 14].

In this study, we also assessed the potential increase in d' from using a TF for our ULD protocols. Since 2016, ULD protocols for the chest (C-ULD), lumbar-spine and pelvis/ hip (S-ULD) have been routinely used in the emergency room [7; 9; 10]. These protocols have many clinical applications with dose levels similar to radiographic examinations. However, the image quality is degraded and requires adaptation, particularly for junior radiologists [6; 7; 10]. The results found in this study demonstrated that using a TF improved d' values for C-ULD for both modeled lesions and for both Sn100 kVp and Sn150 kVp. For S-ULD, the d' values were improved for both simulated lesions only for Sn100 kVp.

Finally, the different results presented in this study showed that the use of Sn100 kVp appeared to be more suitable than Sn150 kVp. A previous study on low-dose non-contrast-enhanced abdominal CT has specified that the use of Sn150 kVp reduced the contrast resolution due to an increase in the Compton effect [13]. The use of Sn100 kVp could, therefore, be used for our various ULD protocols initially to improve the image quality but could later make it possible to reduce doses, especially for the ULD protocols of osteoarticular explorations. Sn150 kVp could be used in addition to Sn100 kVp for overweight patients. Moreover, the use of a tube voltage between Sn100 kVp and Sn150 kVp would make it possible to better adapt the dose and image quality to a patient's morphology. Tube voltages below Sn100 kVp could also be adapted for pediatric patients. Other CT models from the same manufacturer are now equipped with TFs for tube voltages between 100 kVp and 140 kVp (in 10 kVp steps).

This study has several limitations. The raw data were reconstructed using a single iterative level and a single reconstruction kernel. Other combinations of parameters may have produced different outcomes. We evaluated only four task functions, which were not representative of the range of tasks that must be performed in clinical practice. Finally, we used an image quality phantom, and the results might have been different on patients.

In conclusion, the use of a TF improves the X-ray beam quality and also improves the noise characteristics, spatial resolution and detectability indices. The use of Sn100 kVp could be used for our various ULD protocols initially to improve the image quality but subsequently used to reduce the doses, especially for the osteoarticular ULD protocols. Further clinical study should be performed to validate the results found in this phantom study.

Conflicts of interest

The authors have no conflicts of interest to disclose in relation with this article.

Acknowledgments

REFERENCES

1   Brenner DJ, Hall EJ. Computed tomography--an increasing source of radiation exposure. N Engl J Med 2007; 357:2277-84

2   Greffier J, Larbi A, Frandon J, Moliner G, Beregi JP, Pereira F. Comparison of noise-magnitude and noise-texture across two generations of iterative reconstruction algorithms from three manufacturers. Diagn Interv Imaging 2019; 100:401-10

3   Greffier J, Macri F, Larbi A, Fernandez A, Pereira F, Mekkaoui C, et al. Dose reduction with iterative reconstruction in multi-detector CT: what is the impact on deformation of circular structures in phantom study? Diagn Interv Imaging 2016; 97:187-96

4   Greffier J, Pereira F, Macri F, Beregi JP, Larbi A. CT dose reduction using automatic exposure control and iterative reconstruction: a chest paediatric phantoms study. Phys Med 2016; 32:582-9

5   Katsura M, Matsuda I, Akahane M, Sato J, Akai H, Yasaka K, et al. Model-based iterative reconstruction technique for radiation dose reduction in chest CT: comparison with the adaptive statistical iterative reconstruction technique. Eur Radiol 2012; 22:1613-23

6   Larbi A, Orliac C, Frandon J, Pereira F, Ruyer A, Goupil J, et al. Detection and characterization of focal liver lesions with ultra-low dose computed tomography in neoplastic patients. Diagn Interv Imaging 2018; 99:311-20

7   Macri F, Greffier J, Khasanova E, Claret PG, Bastide S, Larbi A, et al. Minor blunt thoracic trauma in the emergency department: sensitivity and specificity of chest ultralow-dose computed tomography compared with conventional radiography. Ann Emerg Med 2019; 73:665-70

8   Samei E, Richard S. Assessment of the dose reduction potential of a model-based iterative reconstruction algorithm using a task-based performance metrology. Med Phys 2015; 42:314-23

9	Greffier J, Frandon J, Pereira F, Hamard A, Beregi JP, Larbi A, et al. Optimization of radiation dose for CT detection of lytic and sclerotic bone lesions: a phantom study. Eur Radiol 2019; doi: 10.1007/s00330-019-06425-z

10	Macri F, Greffier J, Pereira F, Rosa AC, Khasanova E, Claret PG, et al. Value of ultra-low-dose chest CT with iterative reconstruction for selected emergency room patients with acute dyspnea. Eur J Radiol 2016; 85:1637-44

11	Gordic S, Morsbach F, Schmidt B, Allmendinger T, Florh T, Husarik D, et al. Ultralow-dose chest computed tomography for pulmonary nodule detection: first performance evaluation of single energy scanning with spectral shaping. Invest Radiol 2014; 49:465-73

12	Lee SM, Choo HJ, Lee SJ, Kim SK, Lee IS, Kim DW, et al. Cervical spine CT using spectral shaping: can it be a solution to overcome artifacts in the lower cervical spinal region? Korean J Radiol 2019; 20:469-78

13	Leyendecker P, Faucher V, Labani A, Noblet V, Lefebvre F, Magotteaux P, et al. Prospective evaluation of ultra-low-dose contrast-enhanced 100-kV abdominal computed tomography with tin filter: effect on radiation dose reduction and image quality with a third-generation dual-source CT system. Eur Radiol 2019; 29:2107-16

14	Mozaffary A, Trabzonlu TA, Kim D, Yaghmai V. Comparison of tin filter-based spectral shaping CT and low-dose protocol for detection of urinary calculi. AJR Am J Roentgenol 2019; 212:808-14

15	Suntharalingam S, Mikat C, Wetter A, Guberina N, Salem A, Heil P, et al. Whole-body ultra-low dose CT using spectral shaping for detection of osteolytic lesion in multiple myeloma. Eur Radiol 2018; 28:2273-80

16	Poludniowski G, Landry G, DeBlois F, Evans PM, Verhaegen F. SpekCalc: a program to calculate photon spectra from tungsten anode x-ray tubes. Phys Med Biol 2009; 54:N433-8

17   Richard S, Husarik DB, Yadava G, Murphy SN, Samei E. Towards task-based assessment of CT performance: system and object MTF across different reconstruction algorithms. Med Phys 2012; 39:4115-22

18   Burgess AE, Li X, Abbey CK. Visual signal detectability with two noise components: anomalous masking effects. J Opt Soc Am A Opt Image Sci Vis 1997; 14:2420-42

19   Burgess AE, Wagner RF, Jennings RJ, Barlow HB. Efficiency of human visual signal discrimination. Science 1981; 214:93-4

20   Eckstein M, Bartroff J, Abbey C, Whiting J, Bochud F. Automated computer evaluation and optimization of image compression of x-ray coronary angiograms for signal known exactly detection tasks. Opt Express 2003; 11:460-75

21   Ishida M, Doi K, Loo LN, Metz CE, Lehr JL. Digital image processing: effect on detectability of simulated low-contrast radiographic patterns. Radiology 1984; 150:569-75

22   Rotzinger DC, Racine D, Beigelman-Aubry C, Alfudhili KM, Keller N, Monnin P, et al. Task-based model observer assessment of a partial model-based iterative reconstruction algorithm in thoracic oncologic multidetector CT. Sci Rep 2018; 8:17734

23   Euler A, Solomon J, Marin D, Nelson RC, Samei E. A third-generation adaptive statistical iterative reconstruction technique: phantom study of image noise, spatial resolution, lesion detectability, and dose reduction potential. AJR Am J Roentgenol 2018; 210:1301-8

24   Solomon J, Mileto A, Ramirez-Giraldo JC, Samei E. Diagnostic performance of an advanced modeled iterative reconstruction algorithm for low-contrast detectability with a third-generation dual-source multidetector CT scanner: potential for radiation dose reduction in a multireader study. Radiology 2015; 275:735-45

25   Ott JG, Becce F, Monnin P, Schmidt S, Bochud FO, Verdun FR. Update on the non-prewhitening model observer in computed tomography for the assessment of the adaptive statistical and model-based iterative reconstruction algorithms. Phys Med Biol 2014; 59:4047-64

FIGURE LEGENDS

Figure 1. Photograph shows half layer value assessment using a dosimeter placed on a support and centered at the CT scanner isocenter.

Figure 2. Graph shows spectra obtained for 100 kVp, 120 kVp, 150 kVp, Sn100 kVp and Sn150 kVp using the software SpekCalc (McGill University; Montreal, Canada).

Figure 3. A, Photograph shows ACR QA phantom phantom (Gammex 464) used in the study. **B**, Image shows ROIs used to compute the mean attenuation (N_{CT}) for the air, bone and acrylic inserts in module 1 of the ACR phantom. **C**, Image shows regions of interest (ROIs) used for the noise power spectrum (NPS) assessment in module 3 of the ACR phantom. **D**, Image shows ROIs used to compute the task-based transfer function (TTF) with the bone and acrylic inserts in module 1 of the ACR phantom.

Figure 4. Graphs show noise power spectrum (NPS) curves obtained with 100 kVp, 120 kVp, 150 kVp, Sn100 kVp and Sn150 kVp for all dose levels with the reconstruction kernel Br40.

Figure 5. Graphs show detectability index (d') values of lytic bone lesion or ground-glass opacity in the lung parenchyma (a), sclerotic bone lesion (b) and high contrast pulmonary lesion (c) obtained with 100 kVp, 120 kVp, 150 kVp, Sn100 kVp and Sn150 kVp for all dose levels with the reconstruction kernel Br40.

**Table 1.** Tube currents (mAs) values used according to the $CTDI_{vol}$ for each tube voltage.

Table 2. Mean attenuation values (HU) obtained for all tube voltages and for the reconstruction kernel Br40.

Table 3. Values of peak noise power spectrum (NPS) and mean NPS spatial frequency obtained for all tube voltages and for the reconstruction kernel Br40.
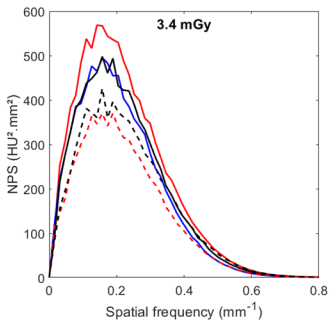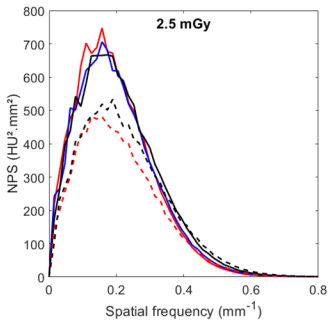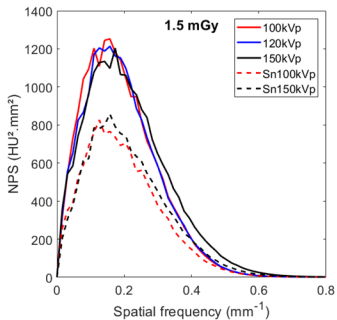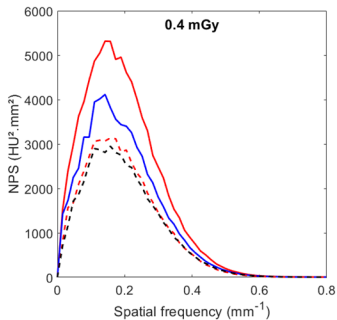
Table 4. Values of task-based transfer function ($TTF_{50\%}$) obtained for acrylic and bone inserts for all tube voltages and for the reconstruction kernel Br40.
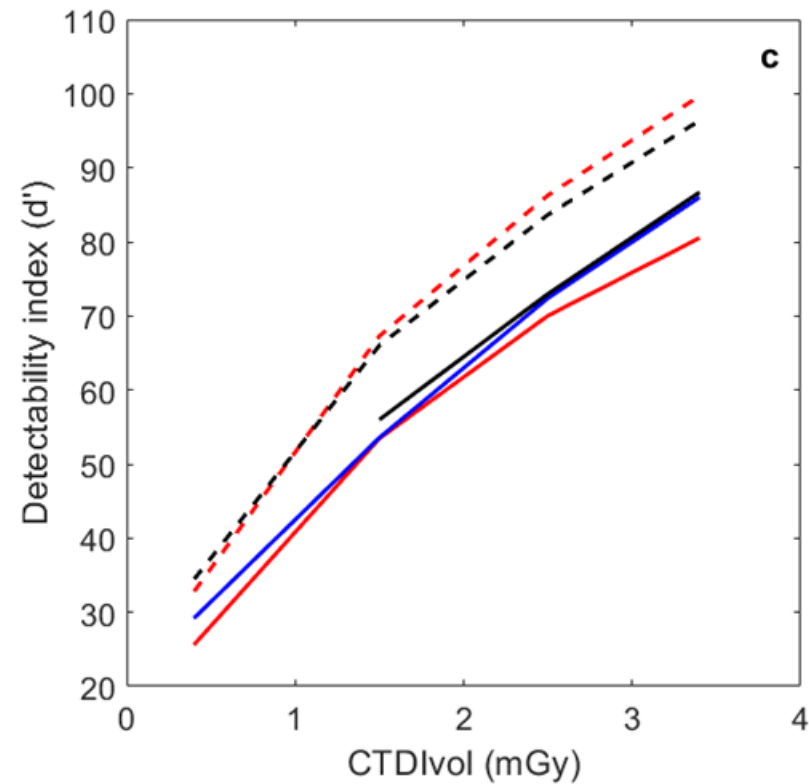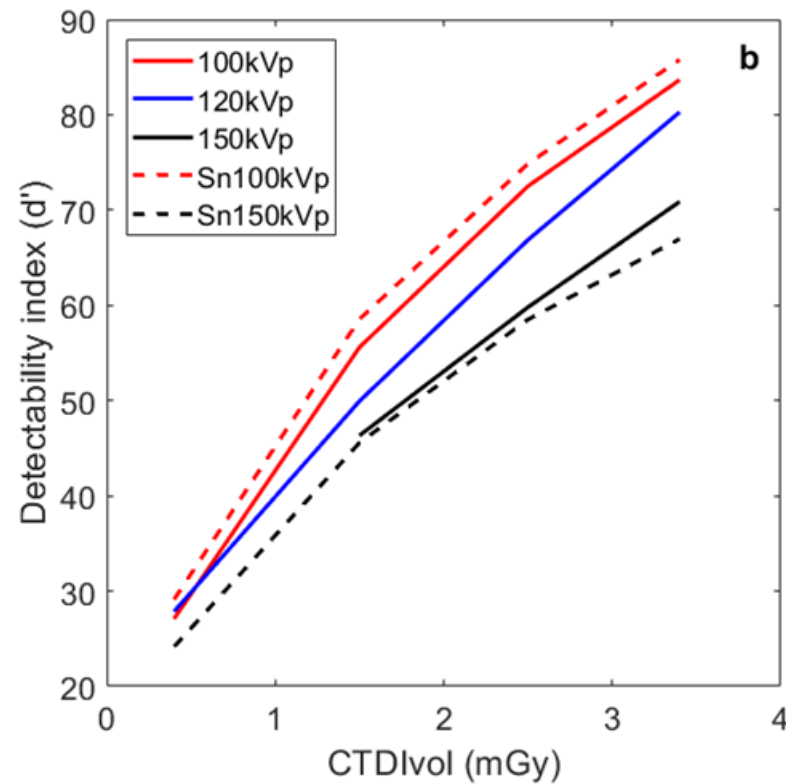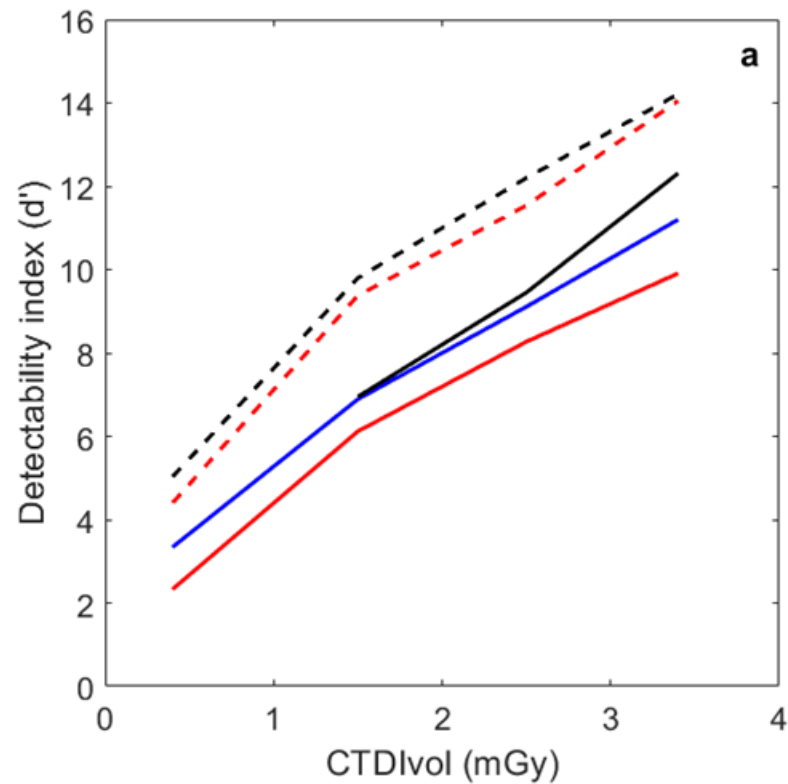
Table 5. Percentage variation for d' ($\Delta d'$) values obtained with Sn100kVp and Sn150kVp compared to those with chest (100kVp) and lumbar spine or pelvis/hips (120kVp) ultra-low dose protocols.

a. b. c. d.
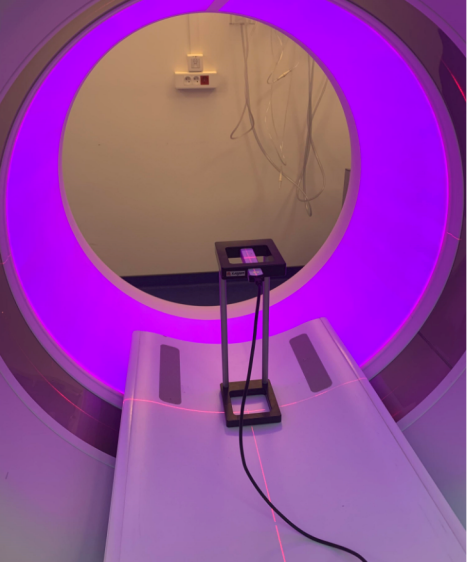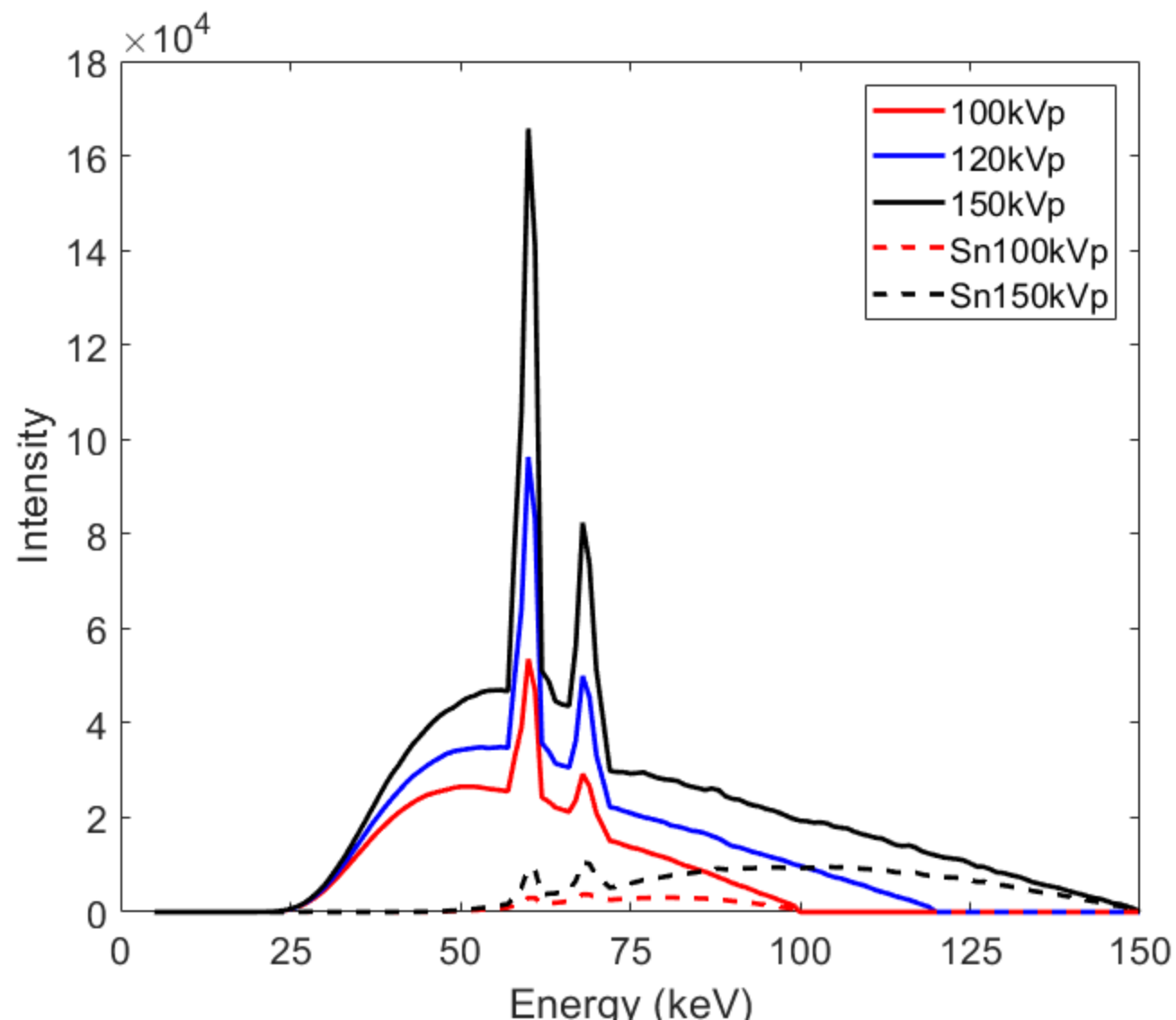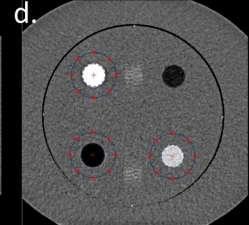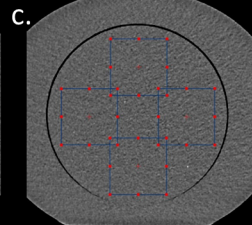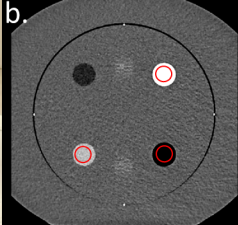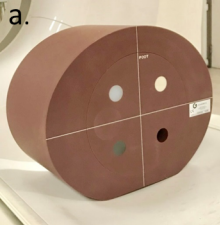
	CTDI$_{vol}$ (mGy)			
Tube voltage	0.4	1.5	2.5	3.4
100kVp	0.37 mGy (10 mAs)	1.52 mGy (38 mAs)	2.49 mGy (62 mAs)	3.41 mGy (85 mAs)
120kVp	0.42 mGy (7 mAs)	1.47 mGy (22 mAs)	2.47 mGy (37 mAs)	3.41 mGy (51 mAs)
150kVp	N.A.	1.49 mGy (13 mAs)	2.52 mGy (22 mAs)	3.40 mGy (32 mAs)
Sn100kVp	0.39 mGy (92 mAs)	1.49 mGy (353 mAs)	2.50 mGy (591 mAs)	3.39 mGy (800 mAs)
Sn150kVp	0.38 mGy (14 mAs)	1.50 mGy (51 mAs)	2.45 mGy (86 mAs)	3.35 mGy (117 mAs)

CTDI$_{vol}$ = volume computed tomography dose index; N.A. = not applicable.

Insert	CTDI$_{vol}$ (mGy)	100 kVp	120 kVp	150 kVp	Sn100 kVp	Sn150 kVp
Bone	0.4	972.0	868.2	N.A.	823.0	639.5
	1.5	971.2	870.6	755.4	805.0	639.0
	2.5	967.3	872.0	753.1	799.5	637.0
	3.4	968.0	869.0	753.4	800.7	639.3
Acrylic	0.4	127.1	130.4	N.A.	133.3	142.3
	1.5	125.8	130.1	136.8	134.3	142.4
	2.5	124.5	129.6	136.5	133.1	143.9
	3.4	125.2	131.2	135.2	132.6	144.3
Air	0.4	-988.9	-985.5	N.A.	-989.1	-978.9
	1.5	-986.6	-990.8	-987.0	-986.7	-988.9
	2.5	-988.2	-987.0	-986.2	-987.6	-988.9
	3.4	-987.9	-987.6	-987.7	-987.2	-988.7

N.A. = not applicable; HU = Hounsfield unit; CTDI$_{vol}$ = volume computed tomography dose index

	CTDI$_{vol}$ (mGy)	100 kVp	120 kVp	150 kVp	Sn100 kVp	Sn150 kVp
NPS peak (HU²·mm²)	0.4	5317	4116	-	3134	3251
	1.5	1253	1214	1203	827	858
	2.5	747	706	667	482	533
	3.4	568	495	498	370	426
Mean NPS spatial frequency (mm^{-1})	0.4	0.19	0.19	-	0.19	0.20
	1.5	0.19	0.19	0.21	0.20	0.21
	2.5	0.20	0.20	0.21	0.21	0.23
	3.4	0.22	0.21	0.22	0.22	0.23

NPS = Noise power spectrum; CTDI$_{vol}$ = volume computed tomography dose index

Insert	CTDI$_{vol}$ (mGy)	100 kVp	120 kVp	150 kVp	Sn100 kVp	Sn150 kVp
Bone	0.4	0.38	0.39	-	0.39	0.42
	1.5	0.38	0.40	0.42	0.40	0.44
	2.5	0.39	0.40	0.43	0.41	0.45
	3.4	0.43	0.41	0.44	0.43	0.46
Acrylic	0.4	0.26	0.36	-	0.31	0.32
	1.5	0.34	0.40	0.40	0.38	0.42
	2.5	0.39	0.42	0.47	0.43	0.50
	3.4	0.44	0.44	0.48	0.50	0.49
Air	0.4	0.32	0.32		0.33	0.33
	1.5	0.32	0.32	0.34	0.33	0.34
	2.5	0.33	0.33	0.35	0.34	0.36
	3.4	0.35	0.34	0.36	0.36	0.38

TTF: Task-based transfer function; CTDI$_{vol}$ = volume computed tomography dose index.

Protocol	Clinical task	Sn100kVp	Sn150kVp
Chest ULD (CTDI$_{vol}$: 0.4 mGy)	Ground-glass opacity (Acrylic insert used)	89 %	51 %
	Pulmonary condensation (Air insert used)	28 %	18 %
Lumbar spine and pelvis ULD (CTDI$_{vol}$: 3.4 mGy)	Lytic bone lesion (Acrylic insert used)	25 %	27 %
	Sclerotic bone lesion (Bone insert used)	7 %	-17 %

ULD = Ultra low dose; CTDI$_{vol}$ = volume computed tomography dose index

Percentage variation of d' values were computed as follows: $\Delta d'(\%) = \frac{d'_{Sn100\ or\ Sn150} - d'_{ULD}}{d'_{ULD}}$